Published online 22 October 2011 *Nucleic Acids Research, 2012, Vol. 40, No. 4* ***1475–1484***
doi:10.1093/nar/gkr866

DNA and nucleosomes direct distinct folding of a linker histone H1 C-terminal domain

He Fang[1], David J. Clark[2] and Jeffrey J. Hayes[1,*]

[1]Department of Biochemistry and Biophysics, University of Rochester Medical Center, Rochester, NY 14625 and [2]Section on Chromatin and Gene Regulation, Program in Genomics of Differentiation, National Institute of Child Health and Human Development, National Institutes of Health, Bethesda MD 20892-2426, USA

Received September 5, 2011; Revised September 26, 2011; Accepted September 27, 2011

ABSTRACT

We previously documented condensation of the H1 CTD consistent with adoption of a defined structure upon nucleosome binding using a bulk FRET assay, supporting proposals that the CTD behaves as an intrinsically disordered domain. In the present study, by determining the distances between two different pairs of sites in the C-terminal domain of full length H1 by FRET, we confirm that nucleosome binding directs folding of the disordered H1 C-terminal domain and provide additional distance constraints for the condensed state. In contrast to nucleosomes, FRET observed upon H1 binding to naked DNA fragments includes both intra- and inter-molecular resonance energy transfer. By eliminating inter-molecular transfer, we find that CTD condensation induced upon H1-binding naked DNA is distinct from that induced by nucleosomes. Moreover, analysis of fluorescence quenching indicates that H1 residues at either end of the CTD experience distinct environments when bound to nucleosomes, and suggest that the penultimate residue in the CTD (K195) is juxtaposed between the two linker DNA helices, proposed to form a stem structure in the H1-bound nucleosome.

Introduction

Linker histones (H1s) are abundant components of chromatin, present at about one molecule per nucleosome in most metazoans (1). These proteins bind specifically to the surface of nucleosomes and are involved in a myriad of biological processes ranging from stabilizing higher order chromatin structures to playing a direct role in regulating gene expression (2–5). Moreover, H1s interact with a plethora of macromolecular partners, including nucleosomes, DNA, transcription factors and histone chaperones (6). However the exact mechanism(s) by which H1 is involved in these processes and is able to interact with multiple macromolecular partners is still obscure. Clearly, detailed knowledge of how H1 interacts in chromatin is essential to fully understand these major biological processes.

Linker histones typically have a three-domain structure including a short N-terminal domain, a conserved globular domain and an extended C-terminal domain (CTD). While the globular domain directs structure-specific recognition and binding to the nucleosome (2), the lysine-rich C-terminal domain interacts with linker DNA in chromatin is responsible for stabilizing folding of nucleosome arrays into chromatin fibers and is required for high affinity binding to chromatin *in vivo* (2,7,8). The CTD also interacts with numerous protein factors in the nucleus, including selected transcription factors and cyclin-dependent kinases (6,9,10). Furthermore, the SPKK motif found in H1 CTDs has been determined to be an effective naked DNA-binding motif by NMR (11).

Early work showed that the CTD was sensitive to degradation by proteases (12) and did not exhibit signatures of defined structure in aqueous solutions of physiological pH and salts (13). However, consistent with predictions of potential α-helical stretches in the CTD, Clark and co-workers (14) demonstrated that a peptide spanning the H1CTD is unstructured in aqueous solution but attains α-helical character in solvents such as TFE. More recently, FTIR has been used to show that isolated CTD peptides adopt a complicated array of structural elements upon interactions with DNA including α-helical structures, β-structures and turns (9). These data support the idea that the CTD is an intrinsically disordered domain that acquires defined structure upon interaction with macromolecular partners. Indeed, Hansen *et al.* (15) have pointed out that H1 CTDs have sequence content emblematic of this class of proteins. Moreover, they have demonstrated that sequence content, not primary structure within the CTD is important for the chromatin-condensing functionality within this domain (7).

*To whom correspondence should be addressed. Tel; +1 585 273 4887; Fax: +1 585 275 6007; Email: jeffrey_hayes@urmc.rochester.edu

H1 binds to the exterior of the nucleosome where the nucleosome dyad passes through the DNA and reorients the linker DNA into a stem-like structure (16–19). In addition, it is likely that linker histones interact with DNA in other locations within chromatin. For example, avian erythrocytes contain approximately 1.4 linker histone molecules for every nucleosome indicating that some H1s must associate with DNA outside canonical site at the nucleosome dyad (1). Indeed the H1-binding affinity for naked DNA fragments is only a few-fold lower than for the canonical site (20). Moreover, nucleosome-free regions exist at promoters and other locations and it is likely that H1s associate with this and other non-canonical DNA sites during rapid exchange about the nucleus *in vivo* (21,22) and *in vitro* (23). Linker histones bind strongly and cooperatively to naked DNA (24) and a histone H1/DNA reconstituted complex exhibits physical condensation at the same ionic strengths as those required for chromatin (13). Importantly, the H1 CTD is a primary determinant of chromatin-binding affinity in the cell nucleus (25). Thus, it is important to understand how H1 binding to the native nucleosome site and DNA affects CTD conformation.

We used FRET and fluorescence quenching analyses to investigate the structure and interactions of the carboxyl-terminus of H1 upon binding of a linker histone to physiological targets. We find that nucleosome binding induces condensation of the H1 CTD in a manner consistent with adoption of a defined structure. Importantly, the CTD exhibits distinct extents of condensation upon association with nucleosomes compared to naked DNA. In addition, our results indicate that specific residues within the CTD are ensconced by DNA helices, and support proposals that the H1CTD contributes to formation of a nucleosome stem structure with linker DNA.

MATERIALS AND METHODS

Expression and purification of full-length H1

H1(0) from *Xenopus laevis* (here referred to as H1) was expressed in bacterial cells using the plasmid pET3aH1(0)a (26). The coding sequences for H1 CTD mutants were generated by the QuickChange site-directed mutagenesis kit (Stratagene) from this plasmid using the upstream primer GAAATCTGGACGGTGTA AGTAAGGAT, GCCAGTGAGGGCATGCAAGGTA A AG and down-stream primers CTTTAGACCTGCCA CATTCATTCCTA, and GGCCTTCTTTACCTTGCAT GCCCTCA to generate coding sequences for H1 K195C, H1 G101CG195C, H1 T173C and H1 G101CT173C. Proteins were expressed and purified as described previously (26) (Supplementary Figure S1A). The concentration of the purified protein stocks was determined by PAGE and quantitative comparison to H1 standards established by amino acid analysis (8).

DNA fragments for nucleosome reconstitution and FRET

DNA fragments used were generated by digestion plasmid p207-12 (27) with Eco RV to release 207-bp DNA fragments containing the 601-nucleosome positioning sequence. Products were isolated from 0.8% polyacrylamide gels and the DNA ethanol was precipitated.

Nucleosome reconstitution

Reconstitution conditions were empirically optimized by independent adjustment of H3/H4 and H2A/H2B amounts to maximize generation of the mono-nucleosome species. Typically, reconstitution conditions contained 5.0 μg of H3/H4 tetramer, 10 μg of 601 DNA fragment and 5.8 μg of H2A/H2B dimer of reconstitution buffer (10 mM Tris, pH 8.0, 1 mM EDTA, 5 mM dithiotheitol [DTT] and 2 M NaCl) in a in 200 μl total volume. Nucleosomes were reconstituted via standard salt dialysis (26). Two reconstitution reactions were combined (400 μl total) and nucleosomes were purified by sedimentation through 10.0 ml 7–20% sucrose gradients (10 mM Tris–HCl, pH 8.0 and 3 mM EDTA) with ultracentrifugation at $34\,000 \times g$ for 18 h in a Beckmann SW41 rotor at 4°C. Nucleosome fractions (500 μl) were collected in 0.6-ml siliconized tubes pretreated with bovine serum albumin (BSA) (0.3 mg/ml) in TE over-night at 4°C. Fractions were analyzed by electrophoresis on nucleoprotein gels [5% acrylamide, 0.5× TBE (1 × 90 mM Tris base, 90 mM boric acid, 2.5 mM EDTA)], stained with ethidium bromide. (Supplementary Figure S1B). BSA was added to peak fractions to 0.15 mg/ml and samples stored at 4°C to prevent dissociation. The purified nucleosomes were found to be stable for several weeks (Supplementary Figure S1C).

FRET analysis

FRET analysis was performed with the H1(0) double mutant H1G101C/K195C, H1G101C/T173C and the combination of single mutant H1G101C, H1K195C, H1T173C. These proteins were prepared, expressed and purified as described above and cysteines reduced by incubation in 50 mM DTT for 1 h, DTT was removed, and the protein was purified by ion-exchange chromatography and quick-frozen (16). The protein was labeled with either maleimido-Cy3 or maleimido-Cy5, or a 50/50 mix of both according to manufacturer's instructions (Pierce), and excess reagent was removed by another round of chromatography. The labeled proteins were diluted to a concentration of 5–20 nM in 150 μl of H1-binding buffer (10 mM Tris–HCl pH 8.0, 50 mM NaCl, 0.3% BSA) and placed in a siliconized glass cuvette. Emission spectra were recorded with excitation at 515- and 610-nm excitation wavelengths on a Horiba Jobin Yvon FluoroMax-4 spectrofluorometer with 5-nm slit widths in both excitation and emission channels. Spectra were recorded in the absence or presence of 207-bp-gradient-purified mono-nucleosomes or the 207-bp DNA fragment alone (free DNA) as indicated in the figure legends. FRET efficiency was calculated as described (28,29) using maximum peak heights and a value of $\varepsilon A(610) = 161103$ (Cy5), $\varepsilon A(515) = 6078$ (Cy5), $\varepsilon D(515) = 92058$ (Cy3) and $d+ = 1$. For the Cy3-Cy5 pair, we used a base Förster radius (R_0) of 5.4 nm (30), which we employed for calculations related to free H1. Due to fluorophore quenching in the nucleosome and DNA complexes, we calculated an adjusted R_0 5.01 and

4.62 nm, respectively, by estimation of the change in the quantum efficiency of donor (Cy3) fluorescence and the resulting effect on the overlap integral (28). Note that changes in quantum yield of fluorescence of acceptor (Cy5) are taken into account in the calculation of FRET efficiency.

RESULTS

To confirm and extend our previous finding of nucleosome-induced condensation of the H1 CTD, we used FRET to determine the distances between labels located at either end of the CTD and when the downstream fluorophore was located at a more interior position. To this end the double H1 mutants G101C/K195C and G101C/T173C were modified with a 50/50 mixture of Cy3-maleimide and Cy5-maleimiade (Figure 1A) and fluorescence emission spectra measured in the absence or presence of nucleosomes reconstituted on a 207-bp DNA fragment, with excitation at 515 or 610 nm (see 'Materials and Methods' section). In accord with previous work (8), Cy5 fluorescence emission (max ~667 nm) was low when either of the two Cy3/Cy5-labeled H1s were irradiated at 515 nm in the absence of nucleosomes (Figures 1B and C), consistent with the domain being disordered. The calculated FRET efficiencies of the double-labeled proteins in the absence of nucleosomes (Figure 1D) combined with an R_0 for the Cy3/Cy5 FRET pair of 5.4 nm (see 'Materials and Methods' section) indicates a distance between fluorophores attached to G101C and K195C of 8 ± 0.3 nm, consistent with the predicted end-to-end distance of an ~100 aa residue worm-like chain of ~9.0 nm (31). Likewise, the calculated distance between fluorophores attached to G101C and T173C is ~6.2 nm, consistent with the predicted end-to-end distance of a ~73 aa residue disordered domain of ~6.6 nm.

We observed significant increases in FRET upon nucleosome binding for both Cy3/Cy5-labeled G101C/K195C and G101C/T173C; emission from Cy3 (~560 nm) was significantly reduced and emission from Cy5 was increased in both cases. Titrations of nucleosomes into the double-labeled H1s show that FRET efficiency increased with nucleosome concentration until reaching a constant value when the ratio of

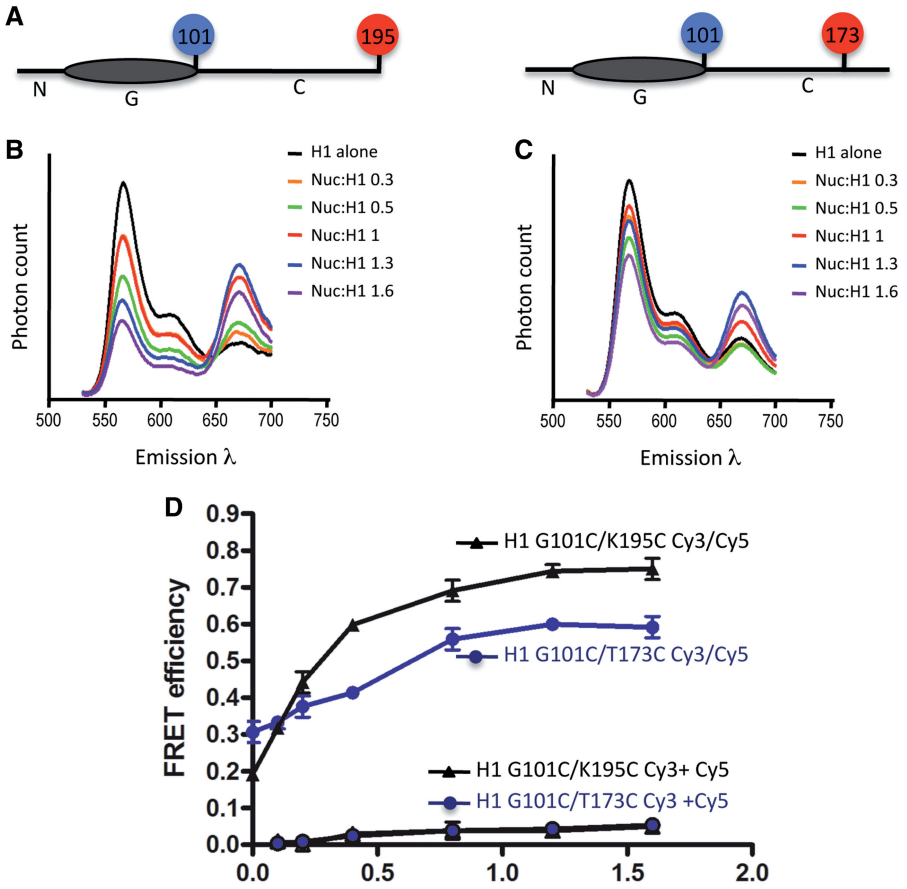

Figure 1. The H1 CTD is intrinsically disordered and condenses upon binding to nucleosomes. (**A**) Schematics of H1 G0101C/K195C (left) and H1 G101C/T173C (right) modified with Cy3 and Cy5 (red and blue). N, G and C denote the N-terminal, globular and C-terminal domains, respectively. (**B**) Binding of Cy3/Cy5-labeled H1 G101C/K195C to nucleosomes results in significant FRET. Emission spectra of 5 nM free H1 (black line) and H1 in the presence of increasing amounts of 207 N nucleosomes, as indicated. Numbers indicate molar ratio of nucleosome:H1. Excitation was at 515 nm. (**C**) As in (**B**) except protein was Cy3/Cy5-labeled H1 G101C/T173C. (**D**) Plot of FRET efficiency as function of nucleosome:H1 ratio for Cy3/Cy5-labeled H1 G101C/K195C and H1 G101C/T173C (filled black triangles and blue circles, respectively, Cy3/Cy5). Also shown are efficiencies for 1:1 mixtures of Cy3- and Cy5-only labeled G101C/K195C and G101C/T173C (triangles and circles, respectively, Cy3+Cy5).

H1: nucleosome was 1:1 or higher (Figure 1D). Thus the maximum FRET efficiency on such plots corresponds to saturated nucleosome binding by H1 in our bulk assays and is used to calculate the distances between labeled sites within the nucleosome-bound form of H1. Interestingly, Cy3/Cy5-labeled G101C/K195C exhibited a greater maximal efficiency in the nucleosome-bound H1 compared to that obtained with Cy3/Cy5-labeled G101C/T173C. The calculated FRET efficiencies of the double H1 mutants indicate a distance between G101C and K195C of 4.2 ± 0.2 nm while the distance between G101C and T173C is 4.9 ± 0.3 nm, consistent with extensive condensation of the CTD domain.

H1 binds strongly and cooperatively to naked DNA and can induce aggregation of samples when present in stoichiometric excess over nucleosomes (20,24). In such complexes, H1s are expected to be located in close proximity; thus there is a possibility that some fraction of the FRET signal in our nucleosome experiments is due to inter-molecular energy transfer. To further characterize the H1 binding in our assays and to ensure that our assays were reporting intra-molecular FRET, a 50:50 mixture of Cy3- and Cy5-only labeled H1s were incubated with nucleosomes. Importantly, these samples exhibited only very low FRET in the absence of nucleosomes and did not exhibit significant increases in efficiencies upon nucleosome binding (Figure 1D). These results indicate that the FRET signal observed with the double-labeled protein in the presence of nucleosomes is solely due to intra-molecular energy transfer.

H1s exhibit rapid mobility about the nucleus and encounter DNA in nucleosome free regions, linker DNA regions and DNA surfaces outside of the defined binding site at the nucleosome dyad (21,22). Therefore it is important to determine whether H1 binding to double-stranded DNA induces CTD folding similar to that observed when binding to nucleosomes. We found that binding of Cy3/Cy5-labeled H1 G101C/K195C to 207-bp DNA fragments resulted in significant FRET (Figure 2A). Cooperative binding of H1 to naked DNA forms oligomeric 'tramtrack' structures and ultimately large rod-like structures (24). Such structures would position several H1 molecules in close proximity, increasing opportunity for inter-molecular resonance energy transfer (Figure 2C). Indeed, titration of DNA fragments into a 1:1 mixture of Cy3-only and Cy5-only labeled H1 G101C/K195C results in significant intermolecular FRET (Figure 2B). Thus, in contrast to nucleosomes, at least a portion of the FRET observed when Cy3/Cy5-labeled H1 G101C/K195C binds to naked 207-bp DNA fragments is due to inter-molecular energy transfer.

Since the FRET observed when Cy3/Cy5-labeled H1 G101C/K195C binds to naked DNA fragments is at least partially due to inter-molecular energy transfer, we wished to quantify the intra-molecular FRET component, if any, to determine whether DNA binding induces CTD condensation. We devised a strategy in which the inter-molecular FRET due to close apposition of neighboring H1 molecules is eliminated by diluting the labeled H1 in the sample with unlabeled protein. We hypothesized that as the ratio of unlabeled:labeled molecules increases, the probability of two labeled molecules being close enough in space to allow for inter-molecular FRET will decrease (Figure 2D). Indeed, in experiments with a 1:1 mix of Cy3- and Cy5-only H1 G101C/K195C, as the ratio of unlabeled H1: labeled H1 increases, the observed (inter-molecular only) FRET decreases until reaching background values (Figure 2E). These data demonstrate that energy transfer between labeled H1s can be decreased and finally be diluted out completely using this method.

We then used the dilution strategy to isolate any intra-molecular FRET caused by folding of H1CTD upon DNA binding. Total FRET was measured for samples containing Cy3- and Cy5-labeled H1 G101C/K195C in the absence and presence of DNA, with increasing ratios of unlabeled: labeled protein. The total observed FRET efficiency in the absence of unlabeled protein was 0.8, significantly higher than that observed for the mix of homogeneously labeled proteins, suggesting an intra-molecular contribution to total FRET. Moreover, upon increasing the ratio of unlabeled: labeled protein, total FRET efficiency decreased, as observed with the mixture of Cy3-H1 and Cy5-H1, until reaching a constant value of 0.33 at 20- to 30-fold dilution (Figure 2E). As we have established that at high dilutions, all inter-molecular FRET has been reduced to 0, this value represents the intrinsic amount of intra-molecular FRET for the H1 CTD within the H1–DNA complex.

Since we observed significant inter-molecular FRET, we next wondered whether the specific labeled sites on the CTD occupied distinct average distances from each other in the cooperatively formed tramtrack structures. To this end, we determined FRET for combinations of singly labeled H1s upon DNA binding (Figure 3). Our results indicate that the labeled sites in all three combinations are within FRET distance from one another in H1–DNA complex and thus all contribute to the observed inter-molecular FRET. Interestingly, since FRET efficiency as indicated by emission by Cy5 (λ max 677 nm, red arrows) is inversely related to fluorophore distance, the shortest distance appears to be between G101C's on adjacent H1s (Figure 3A). In contrast, distances between G101C-K195C and K195C-K195C are somewhat greater (Figure 3B and C). These results suggest that H1s are at least partially arranged in a regular spatial relationship within the tramtrack/rod-like structures.

We noticed in our fluorescence studies different extents of fluorophore quenching upon H1-binding nucleosomes and DNA fragments. Since quenching is dependent upon specific aspects of the fluorophore environment, including proximity to DNA, we further explored the extent of quenching at individual sites in H1 upon nucleosome binding. To simplify the analysis in these experiments we focused on Cy5-labeled proteins since this fluorophore appeared somewhat more susceptible to quenching in our experiments than Cy3 and both exhibited the same relative changes (results not shown). Interestingly, upon binding of Cy5-labeled H1 G101C or H1 K195C to nucleosomes, much greater quenching was observed when the fluorophore was attached to position 195 in H1 compared to position 101 (Figure 4A and B). A plot of the extent of quenching observed upon titration of H1

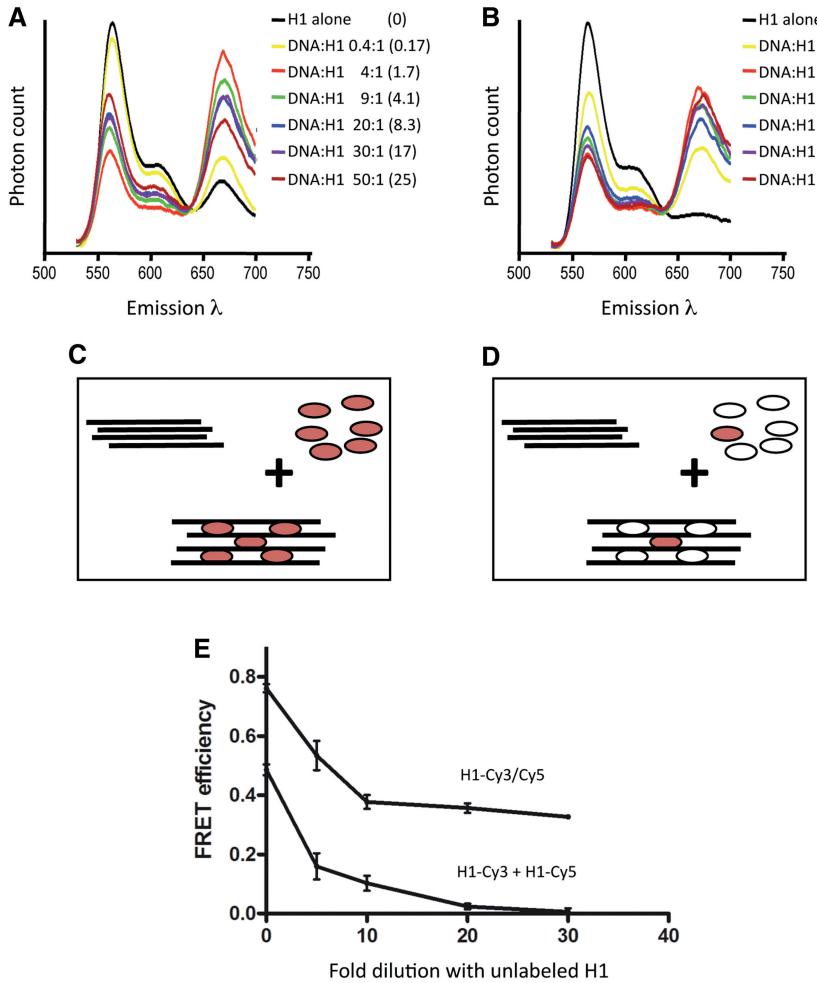

Figure 2. Binding of Cy3/Cy5-labeled H1 G101C/K195C to naked DNA results in both intra- and inter-molecular FRET. (**A**) Binding of Cy3/Cy5 labeled H1 G101C/K195C to naked DNA induces FRET. The protein was incubated alone (black trace) or with increasing amounts of naked 207-bp DNA fragments, as indicated. The molar ratio of DNA:H1 is indicated as is the concentration of DNA in microgram and microliter (in parenthesis). (**B**) Intermolecular FRET upon H1 binding to naked DNA. A 1:1 mixture of Cy3-only and Cy5-only labeled H1 G101C/K195C was incubated alone or in the presence of increasing amounts of 207-bp DNA fragment as in A. (**C**) Schematic of H1–DNA 'tramtrack' structure (24). H1 is indicated by the red ovals; DNA by the lines. (**D**) Model for dilution of inter-molecular FRET with unlabeled H1 (open ovals). (**E**) Elimination of inter-molecular FRET to reveal intra-molecular FRET. Efficiencies for samples prepared as in A (H1-Cy3/Cy5) or B (H1-Cy3 + H1-Cy5) and were determined and plotted (0 point) along with efficiencies for samples in which increasing fractions of the H1 was not labeled with fluorophores.

G101C-Cy5 (Figure 4C) with nucleosomes shows a peak of quenching at lower nucleosome-H1 ratios that was reduced when the H1-nucleosome ratio was 1:1 or greater. We hypothesize that at low nucleosome: H1 ratios, H1 binds nucleosomes at the canonical dyad site but also interacts with nucleosomes in non-specific modes, which contribute more greatly to quenching. At stoichiometric ratios of nucleosomes:H1, where the vast majority of H1 is bound at the dyad site, quenching of the fluorophore at 195 remains high (~0.6) while quenching at 101 is greatly reduced (~0.2). This indicates that the environment surrounding residue 195 is distinct from that surrounding residue 101 when H1 is bound to the nucleosome.

To further investigate the nature of this difference, we examined quenching due to DNA binding by H1 at residues 101 and 195. H1 binds in both cooperative and non-cooperative modes to naked DNA. At the salt concentrations used in our binding studies (50 mM NaCl), the cooperative binding mode is favored, while in buffers of lower ionic strength, a non-cooperative mode is favored (24). Moreover, at high DNA concentrations non-cooperative, distributive binding is expected to increase. We observed that incubation of H1 G101C-Cy5 in the absence or presence of increasing amounts of the 207-bp DNA fragment in 50 mM NaCl resulted in higher fluorescence quenching compared to the same protein incubated with DNA in 20 mM NaCl (Figure 5A). Similarly, when the fluorophore is attached to residue 195, quenching is much higher over the entire range of DNA concentrations in 50 mM NaCl, and compared to that in 20 mM NaCl, with the latter reaching a final value of 0.2 (Figure 5B). This behavior is consistent with the cooperative binding mode being favored at 50 mM NaCl and at lower DNA concentrations, leading to fluorescence

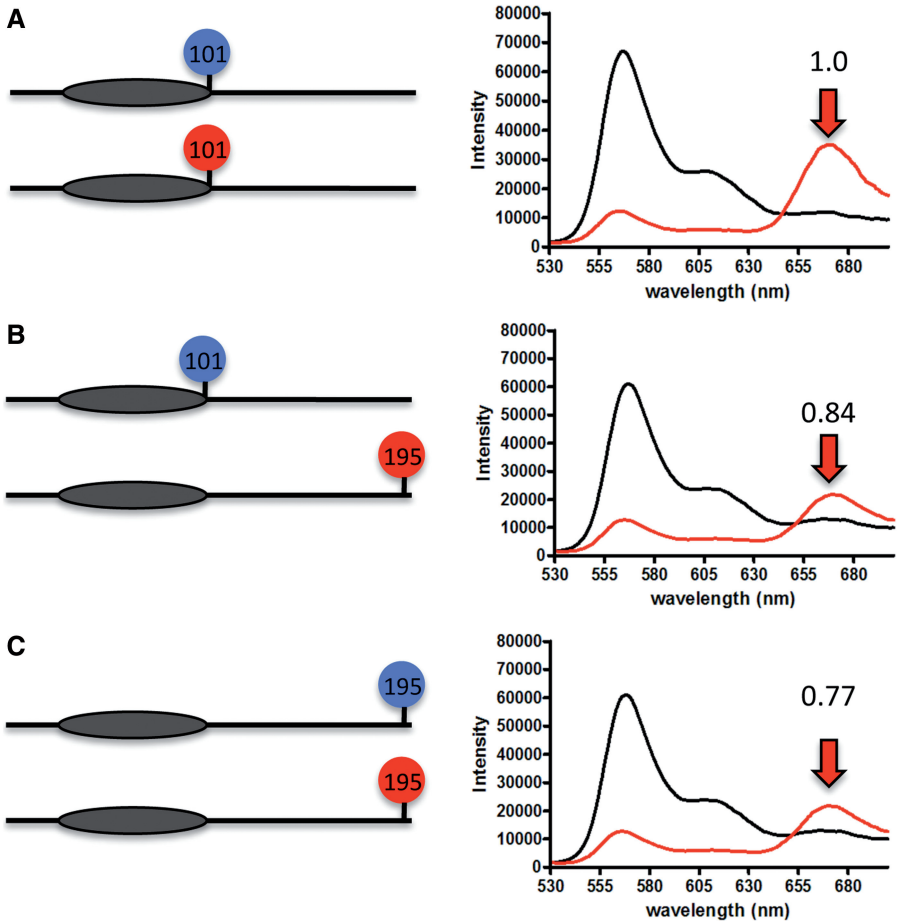

Figure 3. Intermolecular FRET between combinations of labeled sites in H1 upon binding to naked DNA. Pairs of the single substitution mutants H1 G101C and H1 K195C labeled with either Cy3 or Cy5 were mixed in a 1:1 ratio and emission spectra recorded before (black trace) or after (red trace) addition of 207 bp naked DNA fragments. Emission was at 515 nM. (**A**) H1 G101C-Cy3 + H1 G101C-Cy5. (**B**) H1 G101C-Cy3 + H1 K195C-Cy5. (**C**) H1 K195C-Cy3 + H1 K195C-Cy5. The red arrow indicates the Cy5 emission peak. Numbers above the arrow indicate relative FRET efficiency in each experiment.

quenching of ~0.5. In contrast, the non-cooperative mode is favored at high DNA concentrations and 20 mM NaCl, and yields a quenching factor of ~0.2.

DISCUSSION

In this work we confirm and extend previous results demonstrating nucleosome-directed folding of the H1 CTD. Our data strongly support a model whereby the CTD is an intrinsically disordered domain that adopts a specific structure when bound to nucleosomes. Moreover, we find that although H1 binding to DNA induces CTD condensation, this structure is distinct from that formed upon nucleosome interaction. These results indicate that the H1 CTD can adopt numerous structural conformations, as it samples various types of bound and unbound states within the nucleus.

Our data further support the idea that the CTD is intrinsically disordered when H1 is unbound in solution. In the absence of macromolecular-binding partners, distances between specific sites on the H1 CTD are consistent with a disordered polypeptide chain. Specifically, we determined that the distance between residues 101–173 to be ~6.2 nm while residues 101–195 are separated by an average distance of ~8.0 nm, consistent with predicted distances from disordered polymer models (31). Importantly, our measurements indicate that in contrast to the unbound structure, in the nucleosome bound state H1 CTD residues 101 and 195 are closer in space on average than residues 101 and 173. These results provide support for the idea that the CTD condenses into a specific structure upon nucleosome binding and provide important constraints to evaluate models for this structure.

Secondary structure prediction algorithms indicate a high potential for α-helix formation throughout the CTD because alanine and lysine residues are strong helix formers and together account for ~70% of the residues in the CTD of typical H1s (14,32). However, data suggest that α-helices do not form in solution due to repulsions between positively charged lysine residues (33), similar to poly-L-lysine, which forms α-helix if a critical fraction of its charge is neutralized (34). In addition, many H1 CTDs contain numerous internal proline residues, that are

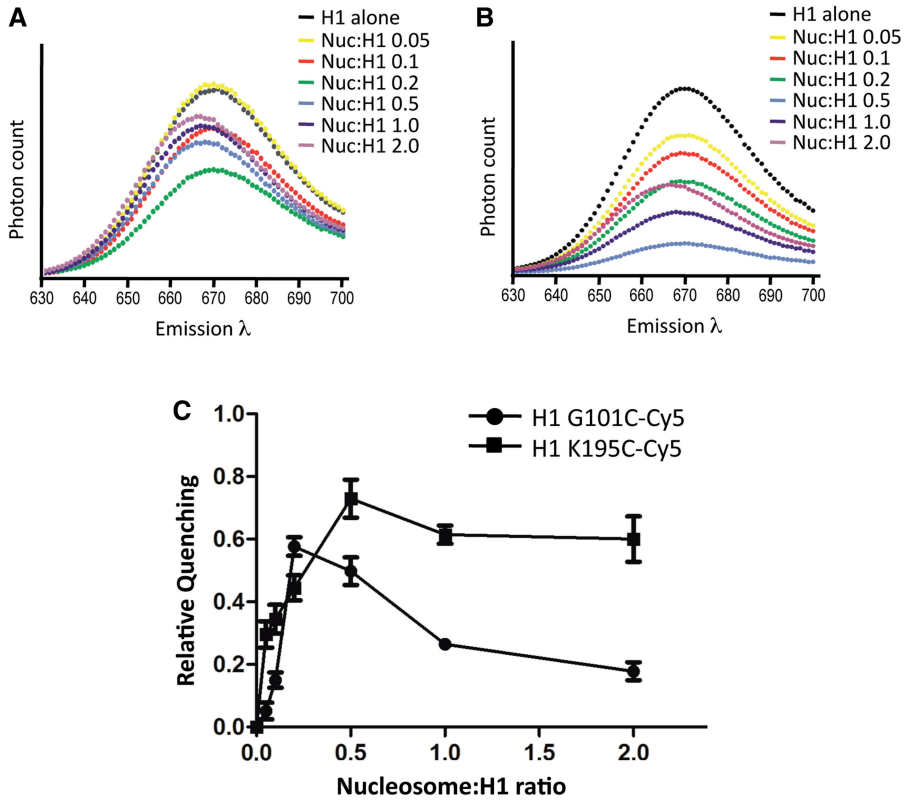

Figure 4. Nucleosome-induced fluorophore quenching is dependent on attachment site. (**A**) Emission spectra of Cy5-modified H1 G101C were recorded in the absence and presence of increasing concentrations of nucleosomes, as indicated. (**B**) As in A except Cy5-H1 K195C was used. (**C**) Plots of the extent of quenching as a function of the nucleosome:H1 ratio. Quenching was determined by the peak height compared to that in the absence of nucleosomes (see 'Materials and Methods' section).

expected to cause kinking of the α-helix into a series of segments. Indeed the H10 CTD used in this study has 13 prolines spaced throughout the domain. In support of this model, the CTD forms α-helix if its charge is partially neutralized or if a solvent favoring hydrogen bond formation is added (14). Interestingly, an H1 from sea urchin sperm that has fewer proline residues can adopt a very long α-helical segment, even when free in solution (35,36). More recent studies have provided direct evidence that α-helix and β-structures are induced in an H1 CTD by binding to DNA (9).

A model for the CTD of rat histone H1d has been proposed based on a combination of sequence analysis, fold recognition and biochemical and biophysical data (37). This model suggests that the H1d-CTD adopts a conformation similar to the HMG-box domain, with the characteristic L- shaped arrangement of helices and an extended N-terminal region. The first two helices form one arm of the L and the third helix and the extended N-terminal region form the other. We aligned our H1 CTD sequence with the H1d CTD and measured the distances between the α-carbons of appropriate amino acids in the model. From our FRET data, the distance between G101 and K195 in the nucleosome-bound protein is 42 Å while the distance between G101 and T173 is 7 Å larger. The model predicts 28 Å between G101 and K195 and a distance between G101 and T173 that is 6 Å larger. Thus our results for the nucleosome-bound H1 are consistent in relative terms but not in absolute distance to this model. Perhaps equilibration with an unfolded form when bound to the nucleosome or orientation of the fluorophores accounts for the difference. It is worth noting that the HMG-box domain is folded in the absence of DNA, unlike the CTD and that normal H1 CTDs have very few of the hydrophobic residues usually required for the formation of a globular fold, whereas such residues are present in the HMG-box domain.

Alternatively, it is possible that different H1 CTDs adopt fundamentally different structures when bound in chromatin. For example, it was originally envisaged that the CTD forms a series of helical segments arranged along the linker DNA, thus guiding and perhaps bending the linker DNA in chromatin (14). As mentioned above a sea urchin sperm H1 has a segment in the CTD that apparently forms a continuous 57 residue α-helix (35,36). The simplest version of this model predicts a very extended structure for the CTD, which seems incompatible with the FRET distance measurements described here. In contrast, the model of the rat H1d CTD mentioned above, while mostly α-helical, predicts a much more compact structure. While this model is qualitatively consistent with our FRET data for *Xenopus* H10, our data are consistent with a more extended model. Compared to normal somatic H1s, the H10 variant and the related H5

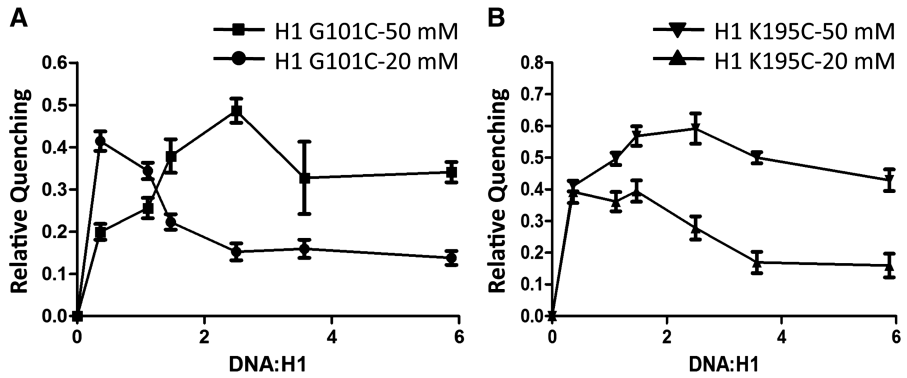

Figure 5. Quenching due to H1 binding naked DNA. (**A**) Quenching of Cy5-H1 G101C fluorescence depends on binding mode. The protein was incubated with increasing amounts of 207 bp naked DNA fragment and the fraction of Cy5 fluorescence quenched determined as compared to fluorescence in the absence of DNA and plotted. Quenching in buffers containing 50 or 20 mM NaCl (cooperative and non-cooperative conditions, respectively) is shown. (**B**) As in A except Cy5-H1 K195C was used.

protein have a significant fraction of alanine residues replaced by valine and isoleucine residues, which are more hydrophobic. Perhaps the CTD of mouse H1d folds into an elongated HMG-box-like structure on binding DNA, whereas the CTD of other H1s adopts a more extended structure because the α-helical segments cannot interact with one another to form a globular domain. It will be interesting in future experiments to compare structures of various H1 CTDs using FRET assays.

In contrast to nucleosomes we find binding to naked DNA resulted in both intra- and inter-molecular resonance energy transfer. We developed a method to isolate FRET due to intra-molecular transfer and discovered binding of H1 to naked DNA resulted in significant folding of the CTD, consistent with previous work showing that CTD peptides adopt secondary structure when exposed to DNA fragments, helix stabilizing solvents and other conditions though to mimic the chromatin environment (9,14,38). However we find that DNA-induced condensation of the CTD is distinct from that induced upon nucleosome binding. FRET experiments indicate DNA binding induces condensation of this domain to a reduced extent compared to that induced upon nucleosome binding, with a distance between residues 101 and 195 in DNA-bound H1 of about 55 ± 3 Å, while we show that these residues are ∼42 Å apart when the protein is bound to nucleosomes (8). In addition, as expected (24), binding to the 207-bp DNA fragment occurs primarily via a cooperative mode, resulting in significant inter-molecule FRET. In contrast no inter-molecular FRET is observed with nucleosomes (Figure 1D).

Our finding of significant inter-molecular FRET in the H1–DNA complex is consistent with the tramtrack model for the H1–DNA complex and provides new details with regard to the disposition of the CTD in this complex. Experiments with singly labeled proteins indicate that all three possible trajectories between residues 101 and 195 on adjacent proteins are within FRET distance. Interestingly, we find evidence that the CTD orientation is not random in the lattice of proteins cooperatively associated with naked DNA fragments. Specifically, we find that residue 101, located between the globular domain and the CTD is closer in space to the same residue on adjacent proteins than it is to residue 195 on adjacent proteins. Moreover, we find that residues 195 on adjacent proteins are also within FRET distance from each other but located further apart than the 101–101 distance.

We also documented quenching of fluorophore fluorescence emission when labeled H1 was bound to nucleosomes. We found that quenching of Cy5 attached to residue 101 is ∼0.2, significantly less than that observed when this fluorophore is attached to residue 195. The extent of quenching observed in the latter case (∼0.6) almost exactly parallels the quenching observed when H1 is associated in a cooperative mode to naked DNA. In this mode, H1 and DNA form 'tramtrack' structures in which two to three DNA strands are likely in close proximity to the fluorophore. In contrast, quenching of fluorophores attached to residue 101, near the globular domain of the protein, is similar in magnitude to that observed when H1 binds in a non-cooperative fashion to naked DNA. In this mode, it is likely that only a single DNA helix is in close proximity to the fluorophore. A model emerges from this analysis whereby a single DNA helix lies in the vicinity of residue 101 when H1 is bound to the nucleosome, while more than one helix is juxtaposed to residue 195. This model is consistent with the C-terminal end of the CTD being located within the stem structure formed by both linker DNA segments, emanating away from the nucleosome along the dyad axis (16–18,39). Recent biophysical analysis and nano-scale modeling of the stem structure indicate a hierarchical structure in which the two linker DNA segments come into close apposition about 20 bp beyond the edge of the nucleosome core region, and intertwine over about 20 bp to form a stem structure with a steep superhelical pitch of about 120 bp (39). Thus, our quenching data suggest that position 195 within C-terminal end of the CTD is located very near or perhaps even within this dual-helix intertwined stem structure, while position 101 is located perhaps closer to the single superhelical gyre at the dyad. It will be of interest in the future to explore exact

spatial relationships between specific positions within the CTD and the chromatosome stem structure.

SUPPLEMENTARY DATA

Supplementary Data are available at NAR online: Supplementary Figure 1A–C.

FUNDING

National Institutes of Health grant [Grant GM52426] (to J.J.H.); the Intramural Research Program of the National Institutes of Health (National Institute of Child Health and Human Development). Funding for open access charge: National Institutes of Health.

Conflict of interest statement. None declared.

REFERENCES

1. Bates,D.L. and Thomas,J.O. (1981) Histones H1 and H5: one or two molecules per nucleosome? *Nucleic Acids Res*., **2**, 5883–5894.
2. Allan,J., Hartman,P.G., Crane-Robinson,C. and Aviles,F.X. (1980) The structure of histone H1 and its location in chromatin. *Nature*, **288**, 675–679.
3. Boulikas,T., Wiseman,J.M. and Garrard,W.T. (1980) Points of contact between histone H1 and the histone octamer. *Proc. Natl Acad. Sci. USA*, **77**, 127–131.
4. van Holde,K.E. (1989) *Chromatin*. Springer Verlag, New York.
5. Shen,X. and Gorovsky,M.A. (1996) Linker histone H1 regulates specific gene expression but not global transcription in vivo. *Cell*, **86**, 475–483.
6. Caterino,T.L. and Hayes,J.J. (2011) Structure of the H1 C-terminal domain and function in chromatin condensation. *Biochem. Cell Biol*., **89**, 35–44.
7. Lu,X., Hamkalo,B., Parseghian,M.H. and Hansen,J.C. (2009) Chromatin condensing functions of the linker histone C-terminal domain are mediated by specific amino acid composition and intrinsic protein disorder. *Biochemistry*, **48**, 164–172.
8. Caterino,T.L., Fang,H. and Hayes,J.J. (2011) Nucleosome linker DNA contacts and induces specific folding of the intrinsically disordered h1 carboxyl-terminal domain. *Mol. Cell. Biol*., **31**, 2341–2348.
9. Roque,A., Iloro,I., Ponte,I., Arrondo,J.L. and Suau,P. (2005) DNA-induced secondary structure of the carboxyl-terminal domain of histone H1. *J. Biol. Chem*., **280**, 32141–32147.
10. Th'ng,J.P., Sung,R., Ye,M. and Hendzel,M.J. (2005) H1 family histones in the nucleus. Control of binding and localization by the C-terminal domain. *J. Biol. Chem*., **280**, 27809–27814.
11. Suzuki,M., Gerstein,M. and Johnson,T. (1993) An NMR study on the DNA-binding SPKK motif and a model for its interaction with DNA. *Protein Eng*., **6**, 565–574.
12. Bohm,L. and Crane-Robinson,C. (1984) Proteases as structural probes for chromatin: the domain structure of histones. *Biosci. Rep*., **4**, 365–386.
13. Puigdomenech,P., Martinez,P., Palau,J., Bradbury,E.M. and Crane-Robinson,C. (1976) Studies on the role and mode of operation of the very-lysine-rich histones in eukaryote chromatin. Nuclear-magnetic-resonance studies on nucleoprotein and histone phi 1-DNA complexes from marine invertebrate sperm. *Eur. J. Biochem*., **65**, 357–363.
14. Clark,D.J., Hill,C.S., Martin,S.R. and Thomas,J.O. (1988) Alpha-helix in the carboxy-terminal domains of histones H1 and H5. *EMBO J*., **7**, 69–75.
15. Hansen,J.C., Lu,X., Ross,E.D. and Woody,R.W. (2006) Intrinsic protein disorder, amino acid composition, and histone terminal domains. *J. Biol. Chem*., **281**, 1853–1856.
16. Sheng,S., Czajkowsky,D.M. and Shao,Z. (2006) Localization of linker histone in chromatosomes by cryo-atomic force microscopy. *Biophys. J*., **91**, L35–L37.
17. Syed,S.H., Goutte-Gattat,D., Becker,N., Meyer,S., Shukla,M.S., Hayes,J.J., Everaers,R., Angelov,D., Bednar,J. and Dimitrov,S. (2010) Single-base resolution mapping of H1-nucleosome interactions and 3D organization of the nucleosome. *Proc. Natl Acad. Sci. USA*, **107**, 9620–9625.
18. Furrer,P., Bednar,J., Dubochet,J., Hamiche,A. and Prunell,A. (1995) DNA at the entry-exit of the nucleosome observed by cryoelectron microscopy. *J. Struct. Biol*., **114**, 177–183.
19. Shukla,M.S., Syed,S.H., Goutte-Gattat,D., Richard,J.L., Montel,F., Hamiche,A., Travers,A., Faivre-Moskalenko,C., Bednar,J., Hayes,J.J. *et al*. (2011) The docking domain of histone H2A is required for H1 binding and RSC-mediated nucleosome remodeling. *Nucleic Acids Res*., **39**, 2559–2570.
20. Hayes,J.J. and Wolffe,A.P. (1993) Preferential and asymmetric interaction of linker histones with 5S DNA in the nucleosome. *Proc. Natl Acad. Sci. USA*, **90**, 6415–6419.
21. Lever,M.A., Th'ng,J.P., Sun,X. and Hendzel,M.J. (2000) Rapid exchange of histone H1.1 on chromatin in living human cells. *Nature*, **408**, 873–876.
22. Misteli,T., Gunjan,A., Hock,R., Bustin,M. and Brown,D.T. (2000) Dynamic binding of histone H1 to chromatin in living cells. *Nature*, **408**, 877–881.
23. Caron,F. and Thomas,J.O. (1981) Exchange of histone H1 between segments of chromatin. *J. Mol. Biol*., **146**, 513–537.
24. Clark,D.J. and Thomas,J.O. (1986) Salt-dependent co-operative interaction of histone H1 with linear DNA. *J. Mol. Biol*., **187**, 569–580.
25. Hendzel,M.J., Lever,M.A., Crawford,E. and Th'ng,J.P. (2004) The C-terminal domain is the primary determinant of histone H1 binding to chromatin in vivo. *J. Biol. Chem*., **279**, 20028–20034.
26. Hayes,J.J. (1996) Site-directed cleavage of DNA by a linker histone–Fe(II) EDTA conjugate: localization of a globular domain binding site within a nucleosome. *Biochemistry*, **35**, 11931–11937.
27. Wang,X. and Hayes,J.J. (2008) Acetylation mimics within individual core histone tail domains indicate distinct roles in regulating the stability of higher-order chromatin structure. *Mol. Cell. Biol*., **28**, 227–236.
28. Majumdar,Z.K., Hickerson,R., Noller,H.F. and Clegg,R.M. (2005) Measurements of internal distance changes of the 30S ribosome using FRET with multiple donor-acceptor pairs: quantitative spectroscopic methods. *J. Mol. Biol*., **351**, 1123–1145.
29. Poirier,M.G., Oh,E., Tims,H.S. and Widom,J. (2009) Dynamics and function of compact nucleosome arrays. *Nat. Struct. Mol. Biol*., **16**, 938–944.
30. Ishii,Y., Yoshida,T., Funatsu,T., Wazawa,T. and Yanagida,T.Y. (1999) Fluorescence resonance energy transfer between single fluorophores attached to a coiled-coil protein in aqueous solution. *Chem. Phys*., **247**, 163–173.
31. Tran,H.T. and Pappu,R.V. (2006) Toward an accurate theoretical framework for describing ensembles for proteins under strongly denaturing conditions. *Biophys. J*., **91**, 1868–1886.
32. Subirana,J.A. (1990) Analysis of the charge distribution in the C-terminal region of histone H1 as related to its interaction with DNA. *Biopolymers*, **29**, 1351–1357.
33. Roque,A., Ponte,I. and Suau,P. (2009) Role of charge neutralization in the folding of the carboxy-terminal domain of histone H1. *J. Phys. Chem. B*, **113**, 12061–12066.
34. Greenfield,N., Davidson,B. and Fasman,G.D. (1967) The use of computed optical rotatory dispersion curves for the evaluation of protein conformation. *Biochemistry*, **6**, 1630–1637.
35. Hill,C.S., Martin,S.R. and Thomas,J.O. (1989) A stable alpha-helical element in the carboxy-terminal domain of free and chromatin-bound histone H1 from sea urchin sperm. *EMBO J*., **8**, 2591–2599.
36. Giancotti,V., Russo,E., Cosimi,S., Cary,P.D. and Crane-Robinson,C. (1981) Secondary and tertiary structural differences between histone H1 molecules from calf thymus and sea-urchin (Sphaerechinus granularis) sperm. *Biochem. J*., **197**, 655–660.

37. Bharath,M.M., Chandra,N.R. and Rao,M.R. (2003) Molecular modeling of the chromatosome particle. *Nucleic Acids Res.*, **31**, 4264–4274.
38. Roque,A., Ponte,I., Arrondo,J.L. and Suau,P. (2008) Phosphorylation of the carboxy-terminal domain of histone H1: effects on secondary structure and DNA condensation. *Nucleic Acids Res.*, **36**, 4719–4726.
39. Meyer,S., Becker,N., Syed,S.H., Goutte-Gattat,D., Shukla,M.S., Hayes,J., Angelov,D., Bednar,J., Dimitrov,S. and Everaers,R. (2011) From crystal and NMR structures, footprints and cryo-electron-micrographs to large and soft structures: nanoscale modeling of the nucleosomal stem. *Nucleic Acids Res.*, **39**, 9139–9154.